COBEM 2023 27TH INTERNATIONAL CONGRESS OF MECHANICAL ENGINEERING

ABCM Brazilian Society of Mechanical Sciences and Engineering
27th ABCM International Congress of Mechanical Engineering
December 04-08, 2023, Florianópolis-SC, Brazil

COB-2023-2037
COGENERATION IN A HIGH CONCENTRATION PHOTOVOLTAIC (HCPV) SYSTEM USING MICROCHANNEL HEAT EXCHANGERS FOR HEAT RECOVERY

Rafael S.M. Moreira
Luz E. Peñaranda
Bruno S. dos Reis
Diego Busson
Gabriel O. Rodrigues
Carolina P. Naveira-Cotta
Federal University of Rio de Janeiro Laboratory of Nano, Microfluidics and Microsystems - LabMEMS, Mechanical Eng. Dept., POLI & COPPE/UFRJ, Rio de Janeiro/RJ, Brazil
rafaelsanmartin@mecanica.coppe.ufrj.br, ing.elenap@gmail.com, bussonn@gmail.com, gabrielodst@gmail.com, carolina@mecanica.coppe.ufrj.br

Abstract. *Renewable energy sources have been widely studied lately to reduce global impacts on the environment or even to supply the demand of remote locations. In the present work, were analyzed the potential of cogeneration of a high concentration photovoltaic system (HCPV) by using microchannel heat exchangers (MCHE) in relevant ambient, with different manufacturing material and geometrical designs, for heat recovery. Two flow rates (45 and 60 ml/min) were tested to prove the incidence of this variable in the heat recovery in the solar cell. Were observed that for lower flow rates the thermal recovery efficiency decreases. The results for the analysis of a pair of mono modules, with a straight channel heat exchanger installed, showed that mono modules with passive and active cooling had statistically the same electrical efficiency 9.29% and 9.41%, respectively. However, for the single module with active cooling, there is the recovery energy in the form of heat of 46.84% leading to a more efficient global use, where 56.25% of all available energy in the solar cell is used.*

Keywords: *Energy efficiency, Cogeneration, HCPV, Microchannels, Heat recovery*

1. INTRODUCTION

Solar energy is a crucial and valuable resource for achieving sustainable power production globally. Among the various systems available, concentrated photovoltaic/thermal (CPV/T) hybrid technology shows great promise due to its capability to simultaneously harness both electrical and thermal energy. In photovoltaic/thermal hybrid (PV/T) systems, low grade heat extraction has been successfully demonstrated. By utilizing optical concentrators, the amount of semiconductor material required can be reduced through the concentration of sunlight onto the photovoltaic (PV) cells, resulting in what is known as concentrated photovoltaic (CPV). However, at higher concentrations, the excess energy flux over the PV cell generates significant heat, requiring the implementation of a cooling system. Through active cooling, this heat can be recovered and utilized as useful thermal energy, combining these concepts to maximize the energy output in the form of a CPV/T system (Sharaf and Orhan, 2015). The applications of the extracted thermal energy primarily depend on the outlet temperature. When the heat reaches high temperatures, it can be utilized to replace the heat generated by fossil fuels in industrial applications (Zimmermann et al., 2015). This option is highly favored as it mitigates CO_2 emissions in regions where electrification is challenging. Other uses for this heat include power generation through the organic Rankine cycle, space heating, desalination, absorption cooling for air conditioning, and providing domestic hot water (provided that the outlet temperature is above approximately 60 °C) (Ju, X. et al., 2017) (Hasan et al., 2018). CPV system uses multijunction photovoltaic (MJPV) cells, with smaller semiconductor areas. These cells can reach higher electrical efficiencies, typically around 40% (Sharaf and Orhan, 2018). However, this results in approximately 60% of the energy waste to the environmental as heat. In this context, cogeneration system represents a convenient solution, where the efficiency usually reaches around 80% due to system losses and parasitic loads such as pumping power in the active cooling system or the power consumed by the tracking system (Sharaf and Orhan, 2015). The thermal resistance of the heat sink used in the heat recovery, is a crucial parameter for the cooling system's performance. Microchannel/minichannel cooling designs have been extensively investigated and proven effective for highly concentrated photovoltaic/thermal (HCPV/T) systems. Microchannels provide increased surface area, enhancing heat transfer without generating excessive pumping power cost (Ali et al., 2020).

Microchannel heat sinks are also commonly used in cooling electronic computer chips, as microprocessor heat fluxes are expected to reach 1 kW/cm^2 (Husain et al., 2016). Micro-pin-fin heat sinks are another popular option, offering higher heat transfer rates at higher pressure drops (Jenkins et al., 2017; Vilarrubi et al., 2018). Innovations in microchannel designs often involve channel shape or manifold design improvements (Ju et al., 2018) [11,12].

This work aims to experimentally demonstrate the operational differences between passive and active cooling methods applied to a CPV multijunction solar cell by utilizing microchannel heat sinks in relevant ambient (TRL6). Furthermore, the investigation incorporates the implementation of four distinct geometries within the microchannel heat sinks, allowing for a comprehensive analysis of their respective performance. For this, microchannel heat exchanger and their respective thermo-hydraulic systems were installed in four of eight single HCPV mono modules (MM). This arrangement provides independence for each one of the groups MM/MCHE to work with different proposals of heat exchangers and different operational conditions and at the same time allows to analysis of the solar to thermal and electric conversion gain under equal climatic conditions.

2. MATERIALS AND METHODS

As shown in Figure 1, an HCPV system with 5kWp was installed in order to recover the heat wasted from the solar cells and use this heat to drive a membrane desalination unit, configuring a cogeneration process. In this sense, mono modules are used in the HCPV system to carry out a comparative analysis of several mono cells in a completely independent and simultaneous way, all subject to the same climatic conditions, but being able to work with different proposals of heat exchangers and/or operational conditions and thus allowing the analysis of the gain solar-electric conversion, with and without different proposals for active cooling.

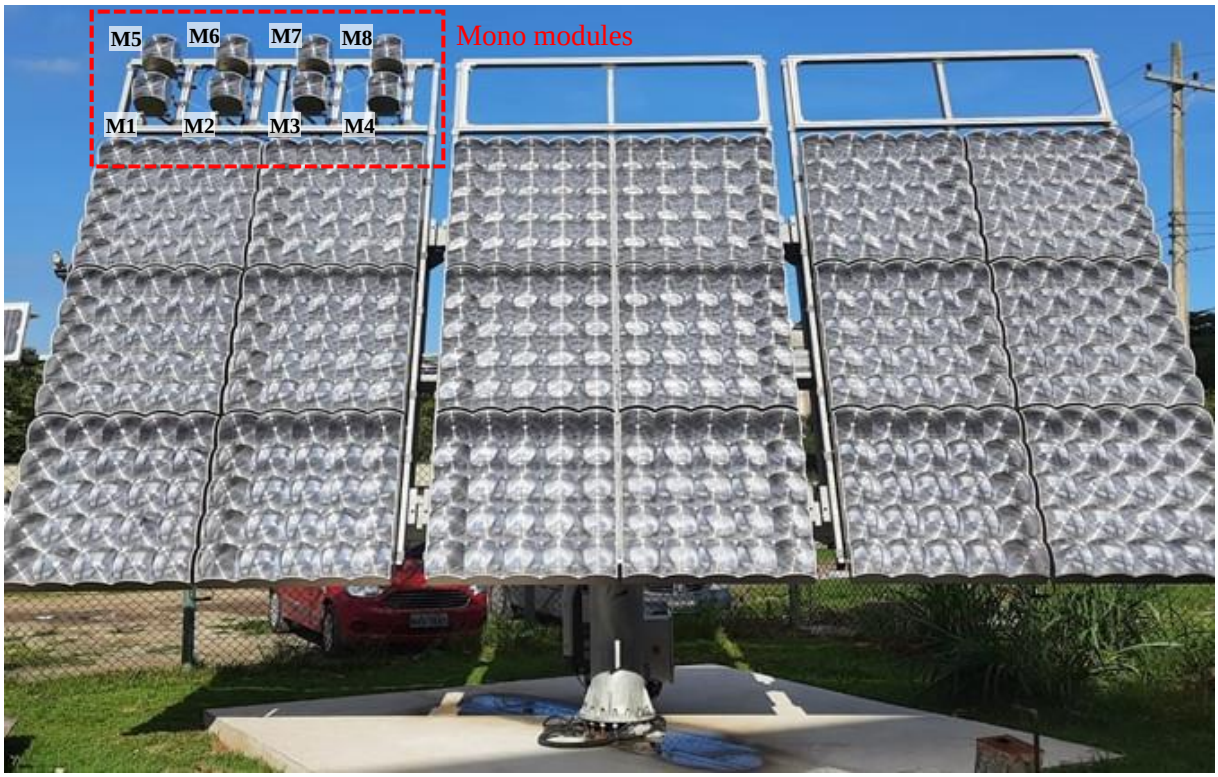

Figure 1. Mono modules used in the HCPV.

The components of the hydraulic circuit of this installation, shown in Figure 2, are contained in a metal box, installed at the back of the grid that supports the mono modules. Also shown is the detail of the components and installation and the micro-channel heatsink. The operation of the evaluation system of microchannel heat exchangers in relevant environment in the mono modules consists of a hydraulic circuit, in which the distilled water used as working fluid is withdrawn from a reservoir through a gear micropump, in a close loop. A micropump was used 24V DC with magnetic coupling and driver controlling the CX-S-0.3-57 reference which has been configured to deliver a maximum flow rate of 75 ml/min for a maximum pressure drop of 10 bar. The controller that has the micropump makes it possible to automatically manipulate the flow rate from a voltage signal provided by the system datalogger. Next, the fluid passes through a particle filter with a 50 µm mesh, then enters the microchannel heat exchanger where the inlet and outlet temperature of the fluid are measured locally, with

type K thermocouples with an uncertainty of 0.2 °C , as well as the pressure drop of the fluid in the heat exchanger for which a differential pressure gauge model PSI.010.DIF from Zurich with a measurement range of 0-1bar and uncertainty of 0.15% is used. After the temperature and pressure measurements, the fluid passes through the cooling system (cooler) to remove the heat gained by the fluid in the heat exchanger in order to avoid overheating the fluid and increasing pressure in the system. Finally, the flow rate is measured using an OMEGA® model FRL1007 turbine meter with a measurement range of 0-100 ml/min and an uncertainty of 1%.

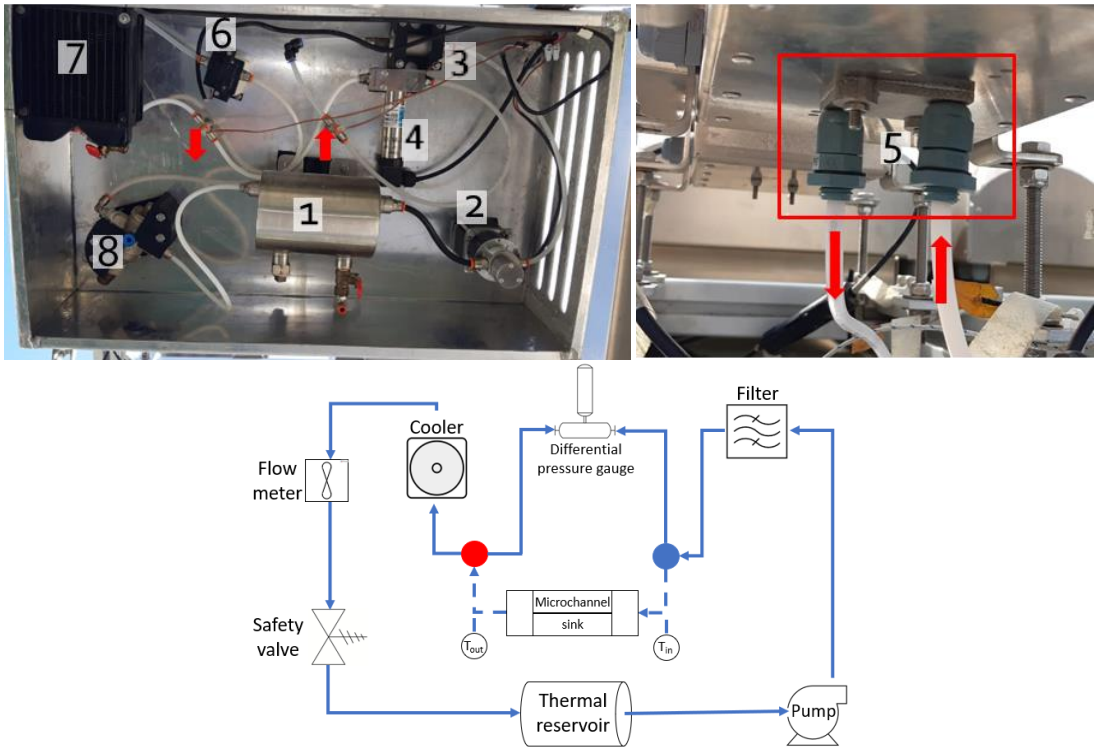

Figure 2. Components of the installed single module hydraulic circuit: (1) Thermal reservoir; (2) Gear micropump; (3) Filter; (4) Differential pressure gauge; (5) Microchannel sink; (6) Flow meter; (7) Cooler; (8) Safety valve

2.1 Microchannel Heat Sink Characteristics

Tests were then carried out on the heatsinks installed on the MM1, MM4, MM6 and MM7 mono modules. The geometry of this microchannel heat exchangers is shown in Figure 3 and the values of the geometric parameters were summarized in Table 1.

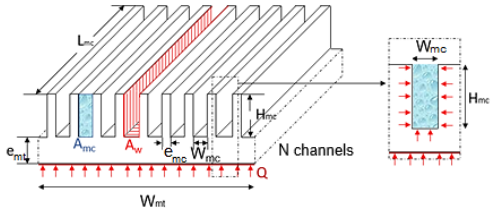

Figure 3. Geometric characteristics of the microchannel heat exchanger.

The heat exchanger implemented in the MM4 single module was optimized as a function of pressure drop, having only 4 straight channels, and whose manufacture was carried out in micromachining using aluminum, while the MM7 single module heat exchanger of straight channels was optimized as a function of the output temperature manufactured via additive manufacturing in Chromium-Cobalt. For the other single modules, a Zig-Zag geometry (MM6) was used and the geometry of straight channels optimized to maximize the outlet temperature manufactured with micro machining in aluminum (MM1). The information with the geometric parameters and manufacturing and material characteristics of the next implementations, were summarized in Table 1.

Table 1. Geometric parameters of installed microchannel heat exchangers.

Description	Notation	MM1	MM4	MM6	MM7
Width of the area occupied by the microchannels	W_{mt} [mm]	20,7	20,7	20,7	20,7
Width of a micro channel	W_{mc} [µm]	900	5000	400	5000
Height of a micro channel	H_{mc} [µm]	1000	4200	1000	4200
Wall thickness between microchannels	e_{mc} [µm]	900	750	400	750
Length of microchannels	L_{mc} [mm]	22,4	22,4	27,6	22,4
Microchannel heat exchanger base thickness	e_{mt} [µm]	800	200	800	200
Number of microchannels in the heat exchanger	N_{mc} [-]	12	4	22	4
Channel type		Straight	Straight	Zig-Zag	Straight
Manufacturing Material		Micro machining Aluminum	Micro machining Aluminum	3D printing CoCrW	3D printing CoCrW
Hydraulic diameter $D_h = \frac{2(W_{mc} \cdot H_{mc})}{W_{mc}+H_{mc}}$	Dh [µm]	947,37	4565,22	642,84	4565,22
Aspect ratio $\alpha = \frac{H_{mc}}{W_{mc}}$	α [-]	1,11	0,84	1,8	0,84
Cross-sectional area of a micro channel	A_{mc} [mm²]	0,90	21,00	0,45	21,00
Total heat exchange area in the microchannels $A_w = N_{mc} \cdot L_{mc}\left(W_{mc} + 2 \cdot H_{mc}\right)$	A_w [mm²]	800,40	1200,64	1748,74	1200,64
Illustrative picture		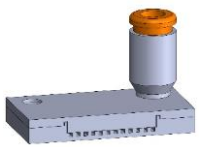	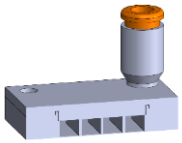	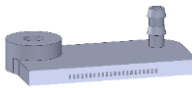	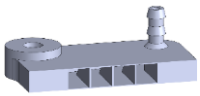

In Table 1, it can be seen that the heat exchangers of the single modules MM1, MM4 and MM7 have channels of rectangular cross-section and straight trajectory, while the heat exchanger of the single module MM6 has a rectangular cross-section, but a zig-zag trajectory as per shown in Figure 4a and Figure 4b, respectively. Zig-Zag heat exchangers are often used in energy-efficient applications because the Zig-Zag design increases the surface area available for heat transfer (see Aw in Table 1), improving heat transfer between fluids circulate in the exchanger. Regarding the Zig-Zag angle, the most common is 45 degrees, but other angles can be used depending on the application. A smaller Zig-Zag angle can increase the surface area available for heat transfer, thus increasing the efficiency of the heat exchanger. However, a smaller angle can also increase the fluid pressure drop, which can reduce the hydraulic efficiency of the exchanger. As shown in Figure 4c, the Zig-Zag angle used for the MM6 single module heat exchanger is 35°. Figure 5 presents a picture of both heat exchangers that were installed in the system.

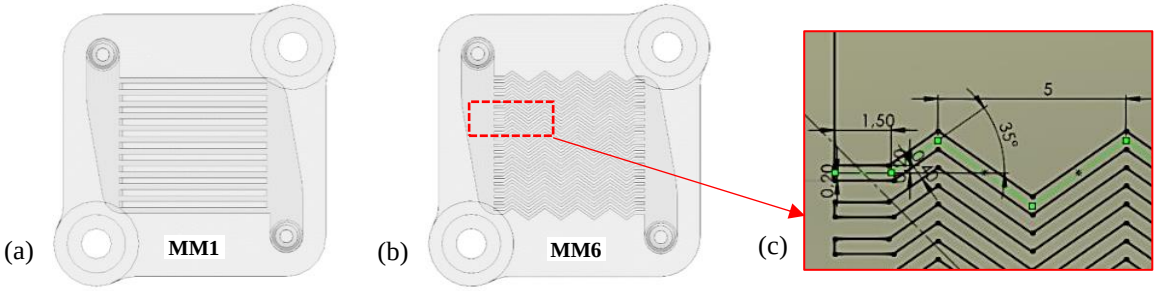

Figure 4. (a) Straight channel heat exchanger; (b) Zig-Zag channel heat exchanger; (c) Detail of the Zig-Zag

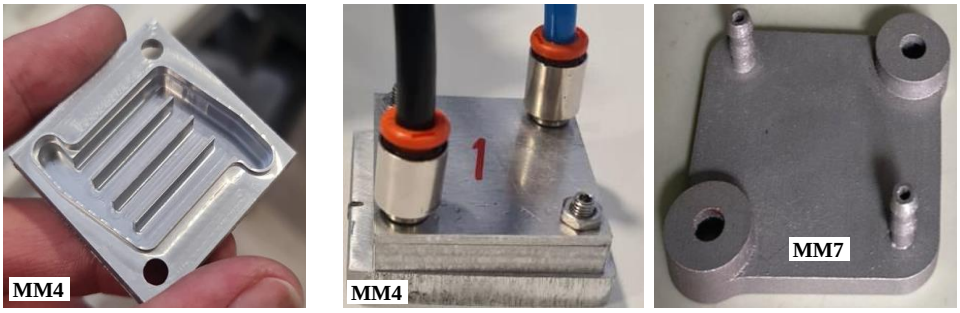

Figure 5. Heat exchangers installed in single modules.

2.2 Thermohydraulic Analysis

The heat gained in the fluid (Q_f) given by the principle of conservation of energy can be expressed as a function of the difference in the average inlet and outlet temperatures as shown in Eq. (1), where ΔT is the average temperature difference at the inlet (T_{in}) and outlet (T_{out}) of the fluid in the microchannel heat sink.

$$Q_f = \dot{m} \cdot c_p \cdot \Delta T \tag{1}$$

The electrical power of the photovoltaic cell can be determined by obtaining the I-V and P-V curves, with the maximum output power obtained by Eq. (2).

$$P_{max} = I_m \,.\, V_m \tag{2}$$

where I_m and V_m is the current and voltage on the maximum power point.

The solar energy that reaches the cell ($E_{available}$) is defined in Eq. (3) by the product of direct solar radiation (DNI), the concentration factor (CR = 820), the solar cell area (A_{cell} = 7mm²) and the optical efficiency of the lens informed by the manufacturer (η_{opt} = 85%).

$$E_{available} = DNI \cdot A_{cell} \cdot CR \cdot \eta_{opt} \tag{3}$$

The electrical efficiency (η_e) of the photovoltaic cell is obtained through the ratio between the maximum power obtained and the available energy:

$$\eta_e = \frac{P_{max}}{E_{available}} \tag{4}$$

Therefore, the thermal efficiency (η_{th}) is given by:

$$\eta_{th} = \frac{Q_f}{E_{available}} \tag{5}$$

3. RESULTS

Among all the experiments carried out, seven days were chosen to exemplify the analysis of the electrical and thermal performance of the monomodules. Figure 6 shows the average of total heat, DNI and inlet and outlet temperatura obtained in these days for two flow rates (45 and 60 ml/min) for a DNI varying between 600-900W/m^2, measured between 10:30h and 14:00h. As can be seen, active cooling in the single module MM4 showed better thermal performance on 04/04 (for a flow rate of 60 ml/min). As for a flow rate of 45 ml/min, the MM1 monomodule obtained the best performance on 24/05 among the analyzed monomodules. It is important to clarify that for a flow rate of 45 ml/min, the data obtained for the MM4 monomodule were inconsistent and therefore it was decided to remove them from the analysis.

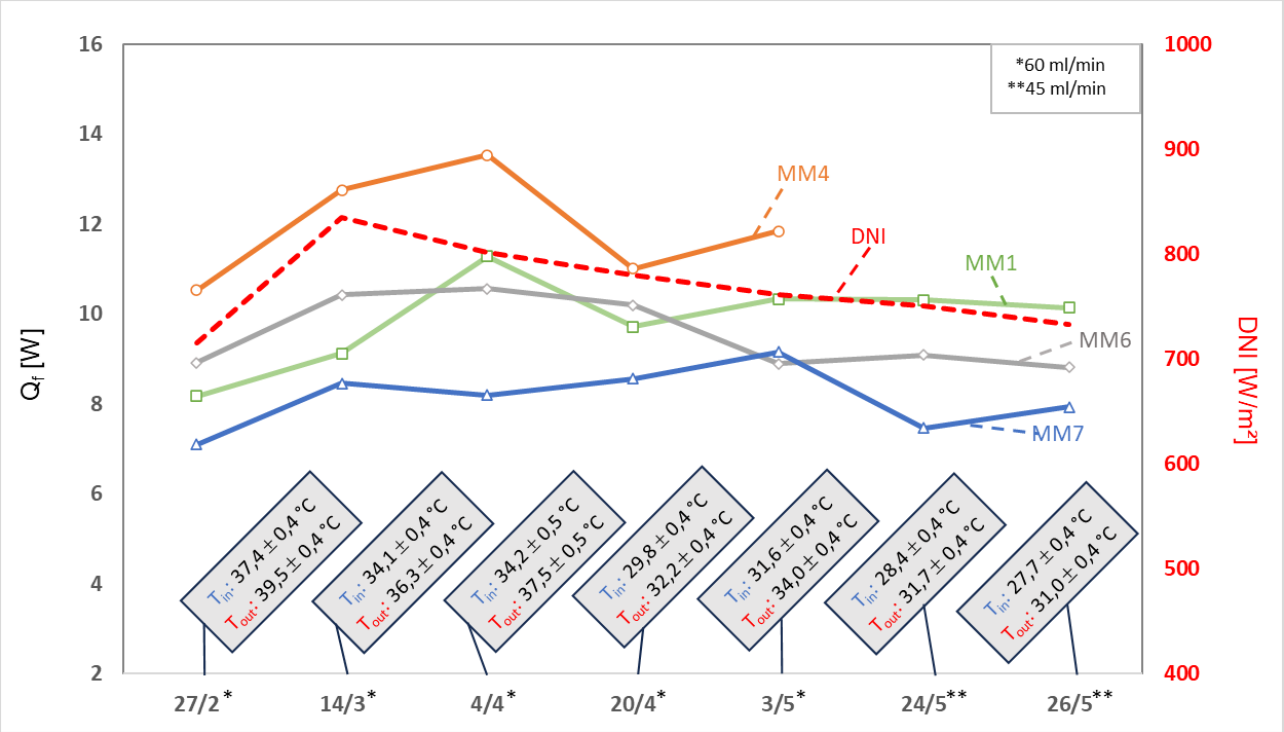

Figure 6. Heat recovered, DNI and inlet and outlet temperature from the system to the exchangers MM1, MM4, MM6 and MM7.

Comparisons for active cooling of the single module MM4 and its corresponding equivalent single module with passive cooling MM3 are presented in Figure 7b, where for a flow rate of 60 ml/min, the best thermal performance was obtained. It can be seen that in relation to electrical generation, the single module with active cooling (MM4) and passive cooling (MM3), presented very close electrical efficiency values, with no statistically significant differences between them.

Analyzing the active cooling of the individual modules, there is a recovery of part of that solar energy that would be lost in the substrates and environment in the form of heat 46.84%. An efficient overall use was obtained, where approximately 56.25% on average of all available energy for the cell can be used. In comparison for the same day and operating condition, Figure 7c shows the energy balance obtained for the MM6 and MM8 single modules. Among the analyzed days, this day the best results were obtained for this geometry. From an electrical point of view, similar efficiency values were also found. As for heat recovery, this geometry showed a drop in relation to the one installed in MM4, with an efficiency of 36.63% (a drop of 10.21%). It is important to point out that the two heatsinks were manufactured with different processes and geometries, which demonstrates the importance of this type of analysis.

For a flow rate of 45 ml/min, the highest heat recovery was obtained for MM1 on 24/05. Figure 7a shows the results obtained, given the operating conditions on that day. As in the other cases, it is possible to observe a similarity in relation to the electrical efficiency between MM1 and MM5. As for heat recovery, a thermal efficiency of 40.14% of all available

energy in the cell was obtained, totaling an overall efficiency of 49.52%. Although each day's operating conditions are different, there is a 6.7% reduction in thermal efficiency compared to the best case obtained for a flow rate of 60 ml/min. As the MM4 and MM1 heatsinks were manufactured by the same method, it can be considered that this drop was due to the flow variation, that is, the greater the flow, the greater the thermal efficiency.

The heatsink installed on the MM7 single module had the lowest heat recovery over all days analyzed. For comparison purposes under the same operating conditions, Figure 7d shows the energy balance obtained on 24/05 for a flow rate of 45 ml/min. Compared to MM1 there was a drop in thermal efficiency of 10.96% (40.14% to 29.18%). Regarding electrical efficiency, there was no significant variation.

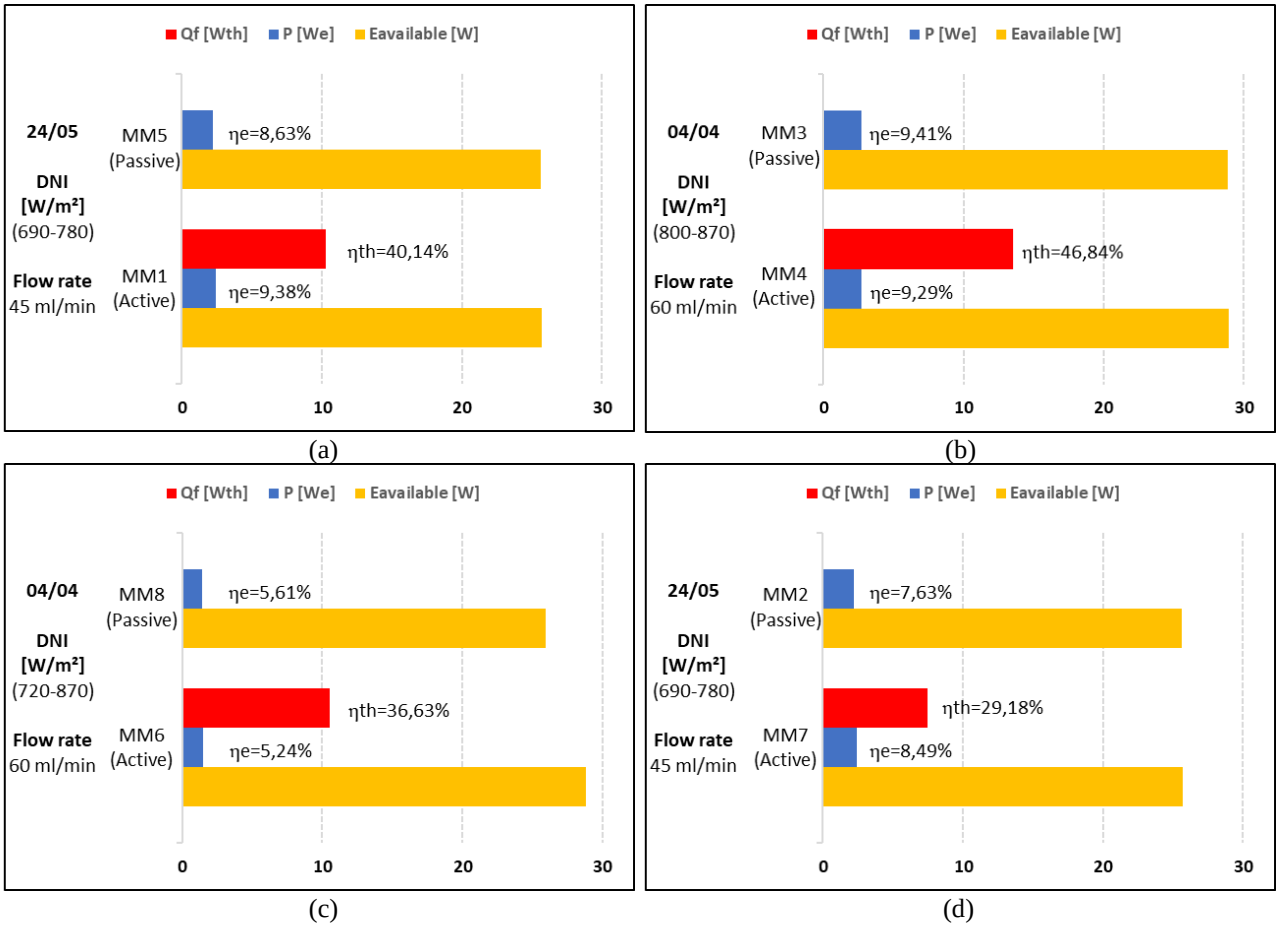

Figure 7. Energy balance with flow rate of 45 and 60 ml/min; time 10:30-14:00; DNI range between 690-870W/m², for the respective active and passive single modules: (a) MM1 and MM5; (b) MM4 and MM3; (c) MM6 and MM8; (d) MM7 and MM2.

4. CONCLUSION

In this study, an experimental comparison between microchannel heatsinks in an HCPV system was performed. The evaluated microchannel sinks present differences in geometry and in the manufacturing process used to produce them. The evaluation methodology was based on energy analysis, including estimates of electrical and thermal efficiency.

A heat exchanger with optimized geometry (4 channels) was manufactured in aluminum through mechanical machining in a microfactory and installed in the single module system (MM4). After comparing the results with heat exchangers of other geometries and manufacturing methods, it was verified that the heat exchanger with optimized geometry and aluminum substrate presented better thermal efficiency results, a variation in thermal efficiency of 10.21% in in relation to the heatsink with zig-zag geometry installed in MM6. However, the heatsink with the same geometry and manufactured with 3D printing (MM7) was the one that obtained the lowest thermal efficiency among all the analyzed ones. With the reduction in flow, a thermal efficiency of approximately 6.7% lower was observed for the heatsink installed in MM1 compared to the experiment with the highest flow (MM4).

In terms of electrical efficiency, the single module with heat exchanger with optimized geometry and aluminum substrate (MM4) also showed a slight gain in relation to the single module with passive cooling.

5. ACKNOWLEDGEMENTS

Partial funding by Petrogal Brasil Project GALP/38, and the sponsoring agencies CNPq, FAPERJ, and CAPES/PROCAD Defesa, are gratefully acknowledged.

6. REFERENCES

Ali, A.Y.M., Abo-Zahhad, E.M., Elqady, H.I., Rabie, M., Elkady, M.F., El-Shazly, A.H. Impact of microchannel heat sink configuration on the performance of high concentrator photovoltaic solar module. Energy Reports, Vol 6, pp. 260-26. 2020.

Çengel, Y. A.; Ghajar, A. J. Transferência de Calor e Massa: uma abordagem prática. 4. ed. 906p. 2012.

Hasan, A., Sarwar, J., Shah, A.H. Concentrated photovoltaic: a review of thermal aspects, challenges and opportunities. Renew Sustain Energy Rev 2018;94: 835–52. https://doi.org/10.1016/j.rser.2018.06.014.

Husain, A., Ariz, M., Al-Rawahi, N.Z.H., Ansari, M.Z. Thermal performance analysis of a hybrid micro-channel, -pillar and -jet impingement heat sink. Appl Therm Eng 2016;102:989–1000. https://doi.org/10.1016/J.APPLTHERMALENG.2016.03.048.

Jenkins, R., Lupoi, R., Kempers, R., Robinson, A.J. Heat transfer performance of boiling jet array impingement on micro-grooved surfaces. Exp Therm Fluid Sci 2017;80:293–304. https://doi.org/10.1016/j.expthermflusci.2016.08.006.

Ju, X., Xu, C., Liao, Z., Du, X., Wei, G., Wang, Z. A review of concentrated photovoltaic-thermal (CPVT) hybrid solar systems with waste heat recovery (WHR). Sci Bull 2017; 62:1388–426. https://doi.org/10.1016/j.scib.2017.10.002.

Ju, X., Xu, C., Zhou, Y., Liao, Z., Yang, Y. Numerical investigation of a novel manifold micro-pin-fin heat sink combining chessboard nozzle-jet concept for ultra-high heat flux removal. Int J Heat Mass Tran 2018;126:1206–18. https://doi.org/ 10.1016/j.ijheatmasstransfer.2018.06.059.

Sharaf, O.Z. and Orhan, M.F. Concentrated photovoltaic thermal (CPVT) solar collector systems: Part I - fundamentals, design considerations and current technologies. Renew Sustain Energy Rev 2015;50:1500–65. https://doi.org/10.1016/j. rser.2015.05.036.

Sharaf, O.Z., Orhan, M.F. Comparative thermodynamic analysis of densely-packed concentrated photovoltaic thermal (CPVT) solar collectors in thermally in-series and in-parallel receiver configurations. Renew Energy 2018;126:296–321. https://doi.org/10.1016/j.renene.2018.03.026.

Vilarrubí, M., Riera, S., Ibanez, M., Omri, M., Laguna, G., Frechette, L. Experimental and numerical study of micro-pin-fin heat sinks with variable density for increased temperature uniformity. Int J Therm Sci 2018;132:424–34. https://doi.org/10.1016/J.IJTHERMALSCI.2018.06.019.

Zimmermann, S., Helmers, H., Tiwari, M.K., Paredes, S., Michel, B., Wiesenfarth, M. A high-efficiency hybrid high-concentration photovoltaic system. Int J Heat Mass Tran 2015;89:514–21. https://doi.org/10.1016/j.ijheatmasstransfer.2015.04.068.

7. RESPONSIBILITY NOTICE

The authors are the only responsible for the printed material included in this paper.